α-Catenin–mediated cadherin clustering couples cadherin and actin dynamics

Chi-Shuo Chen,[1]* Soonjin Hong,[1]* Indrajyoti Indra,[1] Alina P. Sergeeva,[2,3,4] Regina B. Troyanovsky,[1] Lawrence Shapiro,[2,4] Barry Honig,[2,3,4,5] and Sergey M. Troyanovsky[1]

[1]Department of Dermatology, The Feinberg School of Medicine, Northwestern University, Chicago, IL 60611
[2]Department of Biochemistry and Molecular Biophysics and [3]Center for Computational Biology and Bioinformatics, Columbia University Medical Center, New York, NY 10032
[4]Department of Systems Biology, Columbia University, New York, NY 10032
[5]Howard Hughes Medical Institute, Chevy Chase, MD 20815

The function of the actin-binding domain of α-catenin, αABD, including its possible role in the direct anchorage of the cadherin–catenin complex to the actin cytoskeleton, has remained uncertain. We identified two point mutations on the αABD surface that interfere with αABD binding to actin and used them to probe the role of α-catenin–actin interactions in adherens junctions. We found that the junctions directly bound to actin via αABD were more dynamic than the junctions bound to actin indirectly through vinculin and that recombinant αABD interacted with cortical actin but not with actin bundles. This interaction resulted in the formation of numerous short-lived cortex-bound αABD clusters. Our data suggest that αABD clustering drives the continuous assembly of transient, actin-associated cadherin–catenin clusters whose disassembly is maintained by actin depolymerization. It appears then that such actin-dependent αABD clustering is a unique molecular mechanism mediating both integrity and reassembly of the cell–cell adhesive interface formed through weak cis- and trans-intercadherin interactions.

Introduction

Classical cadherins are the principal transmembrane receptors of the polymorphic cell–cell adhesive structures generally known as adherens junctions (AJs). AJs establish tight but highly dynamic contacts between cells in virtually all multicellular tissues. One of the key unanswered questions is whether and how intracellular proteins regulate extracellular cadherin adhesive activity. Although it has been proposed that such inside-out cadherin signaling is based on cadherin oligomerization by the cytoskeleton (Yap et al., 1997; Adams and Nelson, 1998; Kusumi et al., 1999; Gumbiner, 2005), no direct evidence that such a mechanism controls a cell adhesion in vivo has yet been demonstrated.

In recent years, significant progress has been made in understanding the extracellular cell–cell adhesive interface of AJs, which is organized by trans- and cis-intercadherin interactions (Wu et al., 2010; Brasch et al., 2012; Troyanovsky, 2012). Together, these two interactions produce an ordered adhesive structure that interconnects adjacent cells (Harrison et al., 2011). However, these structures, assembled exclusively through cadherin ectodomains, are quite unstable with respect to their lifetimes, morphologies, and mobility of their components. The stability of such ectodomain-based junctions is significantly increased upon their anchorage to the actin cytoskeleton (Hong et al., 2013). Furthermore, cadherin molecules defective for cis-interactions and, therefore, unable to form clusters via their extracellular regions, gain the ability to do so if they interact with actin through a covalently attached actin-binding domain (Hong et al., 2013). These observations suggest that actin filaments can collaborate with extracellular interactions in the formation of AJs. This prompted us to study actin-based mechanisms relevant to cadherin clustering.

Intracellular components of AJs recruit dozens of actin-binding proteins that could in principle participate in cadherin–actin interactions (Kobielak and Fuchs, 2004; Green et al., 2010; Niessen et al., 2011; Ivanov and Naydenov, 2013). Of these, only α-catenin seems to be indispensable. The N-terminal head domain of this protein interacts with cadherin through β-catenin, its C-terminal actin-binding domain (αABD) binds actin filaments, whereas its middle domains (M1, M2, and M3) are thought to control the vinculin-binding site located in the M1 domain (Gomez et al., 2011; Yonemura, 2011). In addition to vinculin, several other actin-binding proteins including EPLIN, ZO1, afadin, α-actinin, spectrin, merlin, and

*C.-S. Chen and S. Hong contributed equally to this paper.

Correspondence to Sergey M. Troyanovsky: s-troyanovsky@northwestern.edu; Barry Honig: bh6@columbia.edu; or Lawrence Shapiro: lss8@columbia.edu

Abbreviations used in this paper: FSM, fluorescent speckle microscopy; SMLM, single molecular localization microscopy; TIRF, total internal reflection fluorescence; TJ, tight junction; wt, wild type.

The Rockefeller University Press $30.00
J. Cell Biol. Vol. 210 No. 4 647–661
www.jcb.org/cgi/doi/10.1083/jcb.201412064

ajuba have been shown to interact with α-catenin (Kobielak and Fuchs, 2004) providing alternative indirect ways for α-catenin to bind F-actin. At least two of these proteins, EPLIN and ZO1, which directly interact with αABD, might constitute alternative linkers between αABD and actin filaments (Imamura et al., 1999; Abe and Takeichi, 2008).

Whether direct αABD binding to actin or alternative indirect mechanisms couple cadherin to actin in AJs is unclear. In vitro binding assays clearly show that β-catenin binding to α-catenin reduces the actin-binding potential of α-catenin (Drees et al., 2005; Yamada et al., 2005), presumably by inhibiting direct αABD–actin interactions. This suggests that αABD, in the context of the cadherin–catenin complex, can interact with actin only if its actin-binding activity is derepressed. On the other hand, there is strong evidence that direct or indirect αABD interaction with actin is an essential step in AJ formation (Pappas and Rimm, 2006; Desai et al., 2013; Thomas et al., 2013) and in initiating a mechanotransduction pathway, resulting in the recruitment of vinculin (Yonemura et al., 2010).

In this study, we explore the role of direct αABD–actin interactions on AJ structure and dynamics. To this end, we identified a set of αABD point mutants unable to interact with actin in vitro. These point mutants allowed us to show that a direct αABD–actin interaction stabilizes AJs, links them to actin filaments, and initiates vinculin recruitment by α-catenin. We also present evidence that AJs connected to actin via αABD, in contrast to those connected to the cytoskeleton through vinculin, are highly dynamic. Exploring the underlying mechanism of these differences in dynamics, we found that αABD binds only to actin filaments located in the cell cortex. This binding, which is transient and cooperative, generates short-lived αABD clusters whose lifetimes are controlled by the turnover of actin filaments. We propose that these transient αABD clusters, formed on cortical actin filaments, facilitate clustering of cadherin molecules and mediate AJ dynamics.

Results

Mutants that disrupt the binding of αABD to actin filaments

αABD consists of a five-helix bundle (residues 671–841) and a C-terminal extension (residues 842–906), which has been seen in two conformations (Ishiyama et al., 2013; Rangarajan and Izard, 2013). In one, the closed conformation, the side chain of the conserved W859 (Fig. S1) inserts into the bundle and the C-terminal extension forms an interface with the bundle. In the open conformation the extension is largely unstructured (Fig. 1 a). It is not known whether either of these is the conformation that binds actin. Previous actin cosedimentation experiments with αABD identified an 18–amino acid–long stretch (residues 865–883) as an actin-binding region (Pappas and Rimm, 2006). Using two recombinant GST fusion proteins, GST-α(671–883), which bound actin, and GST-α(671–864), which failed to bind actin, we confirmed the importance of the 865–883 region in F-actin binding (Fig. 1 b).

A series of three–amino acid alanine substitutions was introduced within the C-terminal extension, and the resulting mutants were tested for interaction with F-actin. These experiments revealed several triple-alanine mutations that significantly decreased this interaction (Fig. 1 c). Four of these mutations were selected for alanine-scanning mutagenesis, which ultimately identified four residues—K842, L852, K866, and L869—that contribute to αABD binding to F-actin (Fig. 1 c). Of these, K866 and L869 are fully exposed in one of the two crystal structures and unstructured in the other. K842 and L852 are buried to a different extent in each structure and, in both cases, link the C-terminal extension to the five-helix bundle. The bundle itself is unlikely to be affected by any of these mutations. Consistently, circular dichroism experiments suggest that the presence or absence of the 866–906 C-terminal region does not impact the overall structure of αABD (Pappas and Rimm, 2006). Collectively, the results suggest that the four residues we have identified are critical to actin binding either through direct contacts or through an indirect structural role in the binding region.

To further characterize a subset of these mutants, we performed F-actin cosedimentation assays with increasing concentrations of αABD and a fixed concentration of F-actin (Fig. 1 d). Curve fitting yielded an apparent K_D for the intact protein of ∼1 μM (Fig. 1 e). This value is close to that previously reported, ∼0.5 μM (Pappas and Rimm, 2006). The K842A mutant showed some evidence of saturation only at its highest concentration, suggesting that its affinity for F-actin is ∼30 μM (Fig. 1 e). The binding affinities of K866A and the deletion mutant GST-α(671–864) were too low to be measured.

Recently, a point mutation, I997A, was identified in the actin binding domain of vinculin that decreases actin binding but has little effect on vinculin folding (Thievessen et al., 2013; Thompson et al., 2014). Because I997 is conserved between vinculin and α-catenin (Fig. S1), we tested the analogous mutant in αABD, I792A. Cosedimentation assays showed that this mutation also significantly decreased binding of αABD to actin (Fig. 1 c). I792 is fairly distant (over 25 Å) from the C-terminal extension; it is buried in an interdomain interface in full-length α-catenin but is exposed on the surface of αABD in isolation (Fig. 1 a).

Having developed mutants that interfere with αABD actin binding, we are now able to assess the role of this interaction in living cells. We chose three of the characterized mutations (K842A, K866A, and I792A) for further experiments.

Direct αABD binding to actin filaments drives junction formation

We first studied the cadherin–α-catenin chimera EcΔ-Dn-α(280–906). The E-cadherin portion of this chimera harbors an extensive cytoplasmic deletion that removes all known intracellular protein binding sites, including the site for p120 (Fig. 2 a). The absence of the latter site, which had not been removed from the cadherin–catenin chimeras used in previous studies (Nagafuchi et al., 1994; Imamura et al., 1999; Desai et al., 2013), excluded an involvement of p120 in any chimera-associated effects. The deleted region was replaced with the photoswitchable fluorescent protein Dendra2 and the C-terminal part of α-catenin (aa 280–906), which includes αABD and all three α-catenin middle domains (M1–M3). The lack of the head domain of α-catenin (aa 1–279) in this chimera simplified data interpretation because it excluded the possibility that this chimera interacted with endogenous β-catenin or underwent homodimerization.

The EcΔ-Dn-α(280–906) chimera produced well-defined intercellular junctions in cadherin-deficient A431D cells (Fig. 2 a), which were very similar in morphology to AJs in wild-type (wt) A431 cells (Indra et al., 2013). Consistent with previous data (Imamura et al., 1999), we found that these junc-

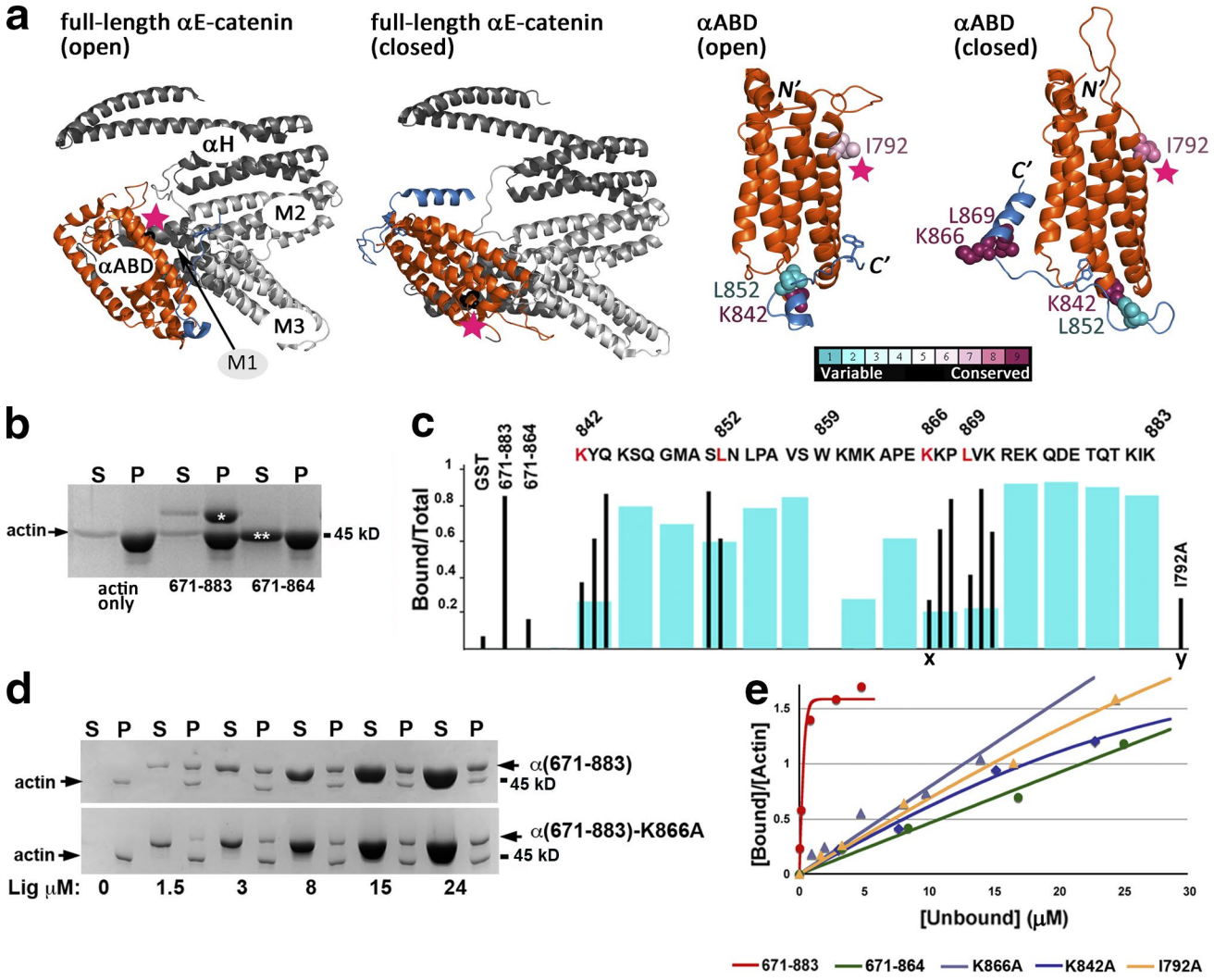

Figure 1. **Characterization of the actin-uncoupled αABD mutants.** (a) Structure of αABD in the context of α-catenin and in isolation in both open and closed conformations (PDB ID 4IGG, chain A and B, respectively). αABD is colored in orange, whereas the other domains of α-catenin (αH, M1, M2, and M3) are in gray. The residues that decrease αABD–actin binding in vitro upon mutation to alanine (Fig. 1 c) are shown as spheres and colored according to conservation score estimated via the ConSurf algorithm (see legend). The conserved W859 is in stick representation. The structurally resolved parts of the C-terminal extension of αABD are colored in blue. I792A is exposed on the surface of αABD in isolation but is buried in the interface between αABD and M1 of full-length α-catenin (pink stars). (b) SDS-PAGE showing the results of actin cosedimentation assays with GST-α(671–883) and its deletion mutant GST-α(671–864), each at 3 μM. Pellet (P) and supernatant (S) fractions are shown. Note that the GST-α(671–883) mutant (one asterisk) cosedimented with the actin filaments, whereas its deletion mutant, GST-α(671–864), marked by two asterisks, remains in the supernatant. Bar shows position of ovalbumin (45 kD). (c) In vitro actin binding assays of αABD mutants. The K842-K883 region of αABD (top line) was divided into triplets, and binding of each triple alanine mutant (blue bars) was plotted as the quantity of mutant protein in the pellet relative to total protein (pellet + supernatant). Based on these data, several point mutations were selected (black bars). For comparison, the binding of control proteins, such as GST, GST-α(671–883), and GST-α(671–864), as well as the point mutant GST-α(671–883)-I792A, is also shown. (d) Cosedimentation assays with GST-α(671–883) and its K866A point mutant at constant F-actin concentration (1 μM) while varying the amount of GST-tagged proteins (ligand [Lig]) from 1.5 to 24 μM. (e) Actin binding curves of GST-α(671–883), GST-α(671–864), GST-α(671–883)-K866A, GST-α(671–883)-K842A, and GST-α(671–883)-I792A. Binding affinities were approximated only for two recombinant proteins that showed evidence of saturation at higher ligand concentrations: K_d(GST-α(671–883)) = 1 μM and K_d(GST-α(671–883)-K842A) = ~30 μM.

tions recruited vinculin and were attached to radial actin bundles, which were integrated with a network of actin bundles connected to other junctions or to focal adhesions (Fig. 2 a). However, when the chimera contained either the K866A or I792A mutations, these junctions were completely abolished (Fig. 2 b). The K842A mutation, which only partially weakened αABD binding to actin in the in vitro assay (see also experiments with Dn-αABD below), did not significantly change the junction-forming properties of the chimera (Fig. 2 b). The correlation between the mutant's abilities to form junctions and their actin-binding affinities suggests that the actin binding site of αABD is essential for the assembly of the chimera's junctions.

The presence of vinculin in the chimera's junctions made it unclear whether αABD continuously anchors the junctions to actin filaments or whether this interaction is transient and is needed only for vinculin recruitment, which then would play the major actin-anchoring function. To clarify this issue, we mutated five key residues of the chimera's vinculin binding site (ΔVin mutation). The resulting chimera still formed actin-associated junctions, which, however, were completely devoid of vinculin

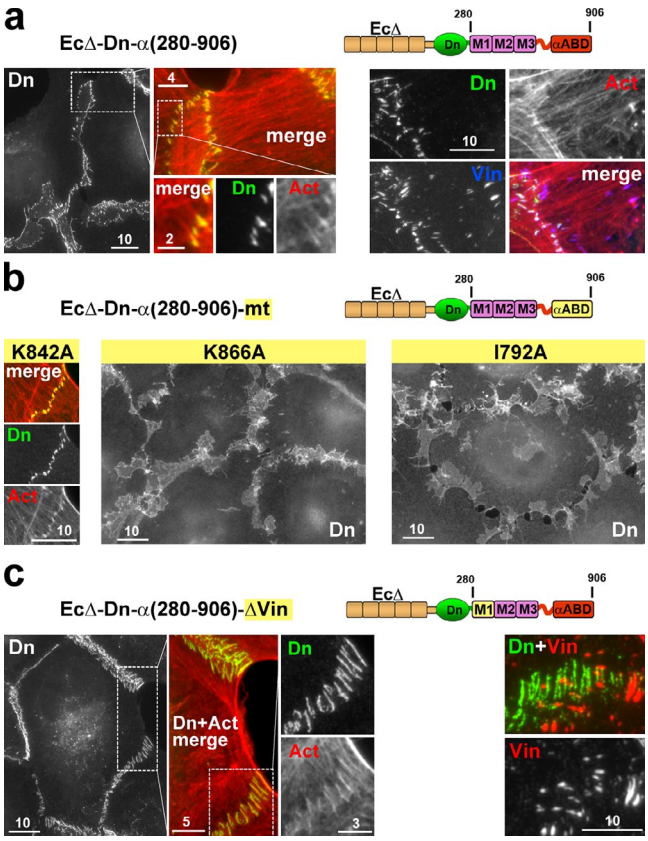

Figure 2. **Direct αABD binding to actin drives junction formation.** (a–c) Immunofluorescence microscopy of cadherin-deficient A431D cells expressing the following chimera molecules: (a) EcΔ-Dn-α(280–906); (b) αABD point mutants (mt) of the EcΔ-Dn-α(280–906) chimera (K842A, K866A, or I792A); and (c) vinculin-uncoupled EcΔ-Dn-α(280–906)-ΔVin mutant. Schematic representation of the chimeras is given atop of the microscopy images. Each chimera includes extracellular, transmembrane, and a 17-aa-long cytoplasmic region of E-cadherin lacking all known cytoplasmic protein binding sites (EcΔ). Dn denotes the fluorescent protein Dendra2. α-(280–906) denotes a region of α-catenin, which includes the M1–M3 domains and the C-terminal actin binding domain (αABD). The mutated domains are in yellow. The dash line boxed regions are magnified on the right or at the bottom. The cells were stained for Dendra2 to reveal chimera (Dn) as well as costained with actin (Dn+Act), vinculin (Dn+Vin), or actin and vinculin together. Expression of EcΔ-Dn-α(280–906)-ΔVin mutant results in formation of actin-enriched junctions devoid of vinculin though actin structures, which are colocalized with chimera are no longer organized into bundles. Numbers above the scale bars indicate micrometers.

(Fig. 2 c). The majority of these junctions were also devoid of ZO-1 and EPLIN (Fig. S2, arrows), thus excluding the possibility that the binding of either of these two proteins participates in indirect interaction of αABD with the cytoskeleton in our ΔVin chimera. Collectively, our data strongly suggest that αABD mediates the direct binding of the EcΔ-Dn-α(280–906) chimera to actin and that this interaction drives junction formation.

Effect of αABD and vinculin on junction morphology

To explore the role of αABD binding to actin in real AJs, we used α-catenin–deficient MDA-MB-468 (468) cells (Figs. 3, 4, 5, 6 and S3). In these cells, E-cadherin forms a complex with β-catenin and p120 that could potentially interact with several actin-binding proteins including vinculin (Hazan et al., 1997; Peng et al., 2010; Ray et al., 2013). Nonetheless, 468 cells cannot form cohesive epithelial sheets (Troyanovsky et al., 2011) or interconnect their numerous E-cadherin lateral clusters with the cytoskeleton (Fig. 3 a). These clusters are likely formed by cis- and trans-extracellular interactions (Harrison et al., 2011) and by p120- or β-catenin–dependent intracellular interactions. The majority of these clusters were devoid of vinculin, EPLIN, and ZO1 (Fig. S3). The lack of detectable association between these clusters and actin allowed us to use 468 cells to investigate the role of αABD in AJs.

Expression of Dendra2-tagged α-catenin (Dn-αCat) in 468 cells restored epithelial organization of their cell–cell contacts including the apicolateral belts of tight junctions (TJs) and AJs (Fig. 3, b and c; and Fig. 4). In addition, the Dn-αCat–reconstituted cells produced two other types of AJs (Fig. 3, b and c) that are also typical of epithelial cells (Takeichi, 2014). Numerous spot-like junctions, variable in their sizes and shapes, formed on their lateral surfaces. These lateral junctions, in contrast to the apicolateral junctions, were devoid of vinculin and were not attached to the phalloidin-positive actin structures (Fig. 3 b). These features are similar to those observed for the lateral cadherin clusters of the parental cells. The third type of junctions, vinculin-containing "basolateral" junctions, was located at the base of the cell–cell contacts. These junctions were symmetrically attached to the actin bundles, which eventually merged with the dense network of stress fibers (Fig. 3, b and c).

We first sought to confirm published data that α-catenin lacking the vinculin binding site is able to form actin-associated AJs (Huveneers et al., 2012; Twiss et al., 2012; Desai et al., 2013). Indeed, 468 cells expressing the ΔVin mutant of α-catenin produced vinculin-deficient junctions, the majority of which were also deficient for ZO1 and EPLIN (Fig. S3). These junctions, still aligned with the robust actin-enriched structures (Fig. 5, a–c), exhibited noticeable defects: the apicolateral AJs as well TJs were fragmented (Fig. 4) and the actin filaments associated with the basolateral junctions were not integrated with the network of stress fibers (Fig. 5 a, basal focus plane). Thus, although α-catenin binding to vinculin is required for normal organization of the AJs, vinculin-deficient AJs, similar to the vinculin-deficient junctions produced by the EcΔ-Dn-α(280–906)-ΔVin chimera, still interact with actin.

Next, we introduced the K866A or I792A point mutations into the α-catenin ΔVin mutant. As expected, the resulting mutants Dn-αCat-ΔVin+K866A (Fig. 5 c) or Dn-αCat-ΔVin+I792A (Fig. 4) associated with the endogenous lateral cadherin clusters because their β-catenin–binding region remained intact. Importantly, morphologically these clusters were indistinguishable from the cadherin clusters of the wt 468 cells (compare Fig. 5 c with Fig. 3 a). Also similar to the parental cells, no actin-enriched structures were detected in association with these clusters (Fig. 5 c) and no TJs were found between these cells (Fig. 4). Basolateral AJs were also undetectable. Such a dramatic effect of the actin-uncoupled αABD point mutations on the ability of the α-catenin ΔVin mutant to assemble AJs provides strong evidence that this protein uses its αABD to directly interact with actin filaments in AJs.

The experiments described in this paper suggest that α-catenin interacts with actin in AJs in two ways: a direct interaction through its αABD or an indirect interaction mediated by vinculin. The α-catenin ΔVin mutant, in contrast, can use only its αABD. To reveal specific properties of AJs linked to actin only through vinculin, we constructed the α-catenin deletion mutant, Dn-αCat(1–505) (Fig. 6 a). Its deletion, (aa 506–906) en-

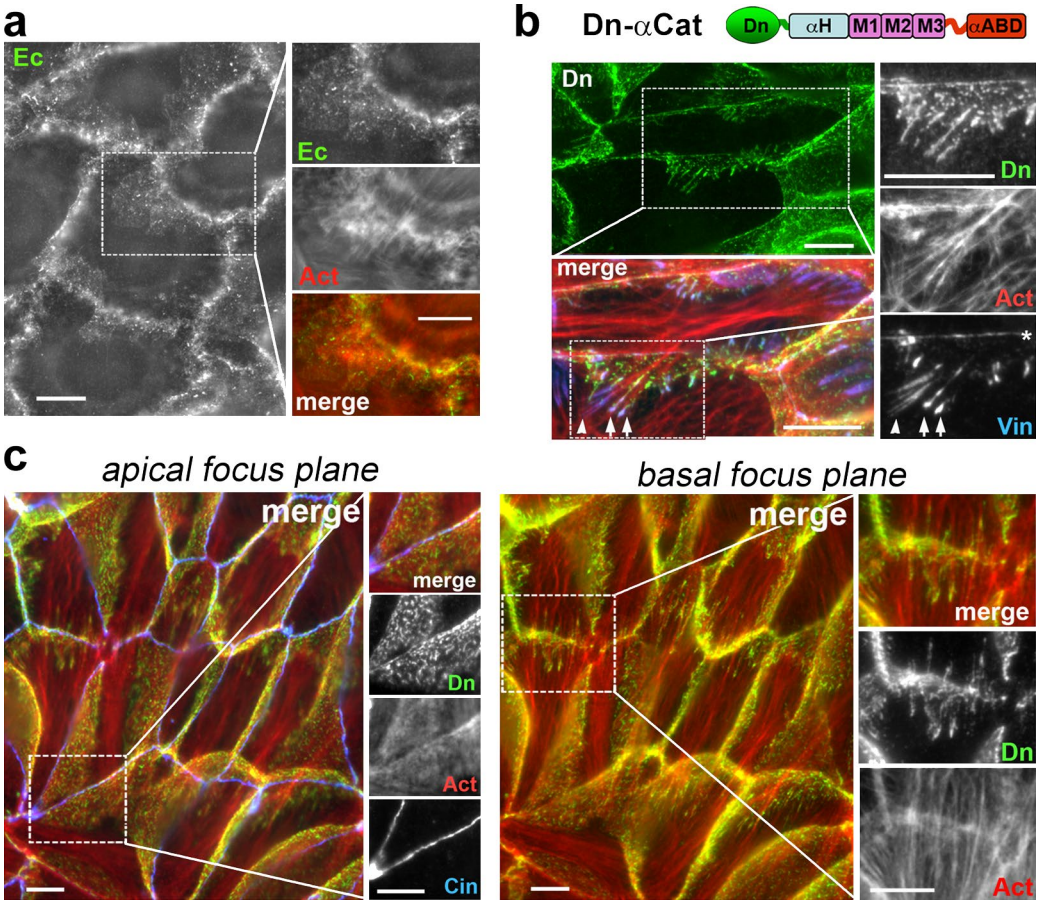

Figure 3. **Polymorphism of AJs in α-catenin–expressing 468 cells.** (a) Immunofluorescence staining of the parental α-catenin–deficient 468 cells for E-cadherin (Ec) and actin filaments (Act). The boxed regions are magnified on the right. Note that E-cadherin molecules can assemble only into tiny clusters. (b) Dn-αCat–expressing 468 cells triple stained for Dendra2 (Dn), actin (Act), and vinculin (Vin). The arrows and the asterisk point to the basolateral and apicolateral junctions, respectively, which are positive for all three markers. The α-catenin–negative focal contacts are indicated by arrowheads. (c) Dn-αCat–expressing 468 cells triple stained for Dendra2 (Dn), actin (Act), and a TJ protein cingulin (Cin). Apical (left) and basal (right) focus planes are shown. Note that the apicolateral AJs associate with TJs and with a fine actin staining (apical focus plane). The lateral cell membranes are enriched with numerous lateral spot-like junctions, which did not show clear association with actin structures. The base of the lateral membranes formed basolateral AJs associated with the radial actin bundles (basal focus plane). Schematic representation of the Dn-αCat is given on the top of image. Dn denotes the GFP Dendra2. αH denotes the head domain of α-catenin implicated in binding to β-catenin and homodimerization. M1–M3 and αABD denote middle domains and αABD of α-catenin, respectively. Bars, 10 µm.

compassing αABD and the M3 domain, permanently activates the vinculin-binding site located in the α-catenin M1 region (Yonemura et al., 2010; Thomas et al., 2013). Consequently, the Dn-αCat(1–505) mutant can interact with actin only or predominantly through association with vinculin. Indeed, this mutant produced vinculin-enriched AJs (Fig. 6 b). Although these junctions clearly associated with actin, their morphology was abnormal: the apicolateral junctions were mostly fragmented (Figs. 4 and 6 a, apical focus plane), and the basolateral junctions, despite forming actin-enriched structures, were dislocated from the actin bundles (Fig. 6 a, basal focus plane). Thus, each of these actin-associated AJs, apicolateral and basolateral, require both vinculin and αABD to achieve their normal morphology.

αABD and vinculin have opposite effects on junction dynamics

Using a Dendra photoconversion assay, we compared the dynamics of the apicolateral junctions formed in 468 cells by intact α-catenin with those formed by Dn-αCat-ΔVin and Dn-αCat(1–505). The results presented in Fig. 6 c reveal remarkable differences. The Dn-αCat-ΔVin–based junctions, connected to actin via αABD only, were very dynamic, losing nearly 30% of their photoconverted fluorescence within 3 min. The junctions formed by the wt α-catenin were slightly more stable. Surprisingly, the Dn-αCat(1–505)–based junctions that were linked to the cytoskeleton through vinculin were extremely stable: their photoconverted fluorescence showed no changes during the same time period. These observations suggest that αABD makes junctions more dynamics, whereas addition of vinculin enhances its strength. In addition, it appears that wt AJs are controlled primarily by αABD-mediated dynamics.

αABD selectively interacts with cortical actin filaments to produce dense clusters

To better understand the role of αABD in AJs, we studied the binding of the Dendra2-tagged αABD (Dn-αABD) to the cytoskeleton in A431 cells. Phalloidin staining showed that this fusion protein decorated cortical actin but not stress fibers or bundles associated with AJs (Fig. 7 a, arrows). This finding was further validated in experiments with Latrunculin A. Its high concentration (4 µM) completely depolymerized the actin cytoskeleton and concomitantly abolished Dn-αABD filamen-

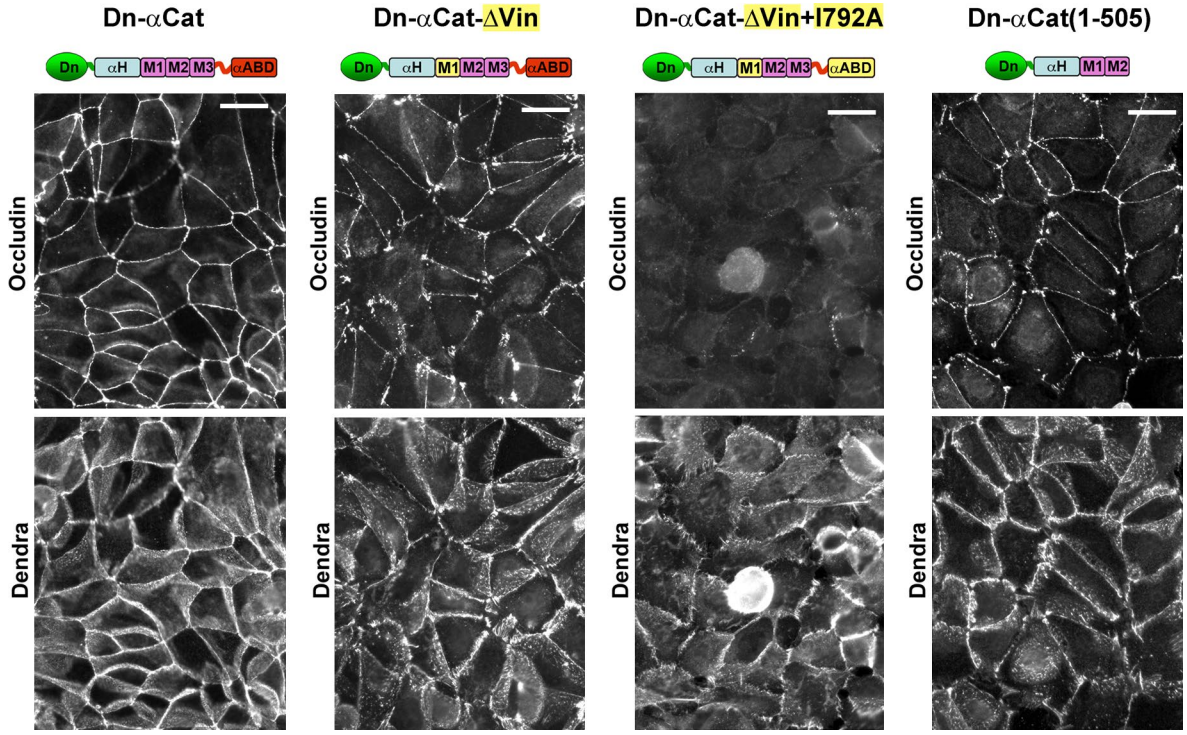

Figure 4. **Comparison of junctions formed by Dn-αCat or its mutants in 468 cells.** The cells were double stained for occludin to reveal TJs (top row) and for Dendra2 to reveal transgene products (bottom row). The maps of Dn-αCat proteins are shown as in Fig. 3. The mutated domains are in yellow. Dn-αCat can interact with actin both directly through αABD and indirectly through vinculin, whereas its Dn-αCat-ΔVin and Dn-αCat(1–505) mutants can only associate with actin specifically through αABD or vinculin, respectively. Both modes of interactions are inactivated in the double mutant Dn-αCat-ΔVin+I792A. Note that cells expressing intact α-catenin were the only ones to produce fully closed rings of TJs. All the mutants showed comparable levels of expression (Fig. S4 a). Bars, 40 µm.

tous organization (Fig. 7 b). At a low concentration (0.4 µM), Latrunculin A left intact some of the bundles. Yet, these bundles remained completely devoid of Dn-αABD, which colocalized with the residual clumps of the cortical filaments (Fig. 7 c). To confirm αABD localization along the actin cortex, we selectively removed actin bundles while maintaining filaments by blocking myosin II activity with Blebbistatin. This treatment did not affect αABD distribution (Fig. 7 d). In the absence of bundles, it became obvious that cortical filaments were not evenly decorated by Dn-αABD, suggesting that some filaments have specific preferences for interactions with αABD.

The K866A or I792A point mutations of αABD completely abolished its association with the cortex (Fig. 7 e). Another mutation, K842A, in contrast, had no obvious effects on Dn-αABD localization. The clearest differences between these proteins were revealed by confocal microscopy: although the intact Dn-αABD was exclusively cortical, its K866A or I792A mutants were cytosolic. The K842A mutant exhibited an intermediate phenotype (Fig. 7 f). Interestingly, the inability of αABD to interact with actin bundles was evident even when recombinant αABD was added to the permeabilized cells (Fig. 7 g).

To increase spatial resolution, we examined the distribution of Dn-αABD using single molecular localization microscopy (SMLM). This technique, which is able to locate individual Dendra2 molecules at 30-nm resolution, confirmed that Dn-αABD does not uniformly bind to the cortex filaments (Fig. 8). Instead, Dn-αABD was localized in numerous clusters. The longest axis of the clusters reached 400 nm and the apparent density of molecules in the cluster reached ~5×10^4 molecules/µm^2 (Fig. 8), consistent with the results of Hansen et al. (2013) who found that actin filaments can be completely covered by αABD. We also imaged cells expressing the Dn-αABD-I792A mutant or Latrunculin A–pretreated cells expressing Dn-αABD. Uncoupling of αABD from actin using either of these techniques dramatically changed cluster appearance: the size of the clusters increased concomitantly with a significant decrease of their molecular density (Fig. 8). The latter value for the majority of the Dn-αABD-I792A clusters was ~2×10^3/µm^2, a ~25-fold reduction from wt values. After latrunculin treatment, the individual clusters were impossible to demarcate.

αABD clusters on cortical actin are short lived

Dn-αABD and its mutants were photoconverted in a small area, and the resulting red fluorescence of the spot was monitored over time. Fig. 9 a shows that the area of its red fluorescence remained constant in size but rapidly decreased in intensity ($t_{1/2}$ = ~10 s). In contrast, the photoconverted spot of its K842A mutant rapidly expanded in size. A drop in red fluorescence of the other two mutants (K866A, I792A) was too fast to be accurately measured. These results suggest that wt αABD remains bound to the same location, whereas the three mutants diffuse away at rates related to their binding properties (Fig. 1 c). The fast decay of wt αABD fluorescence despite its constant spatial localization is consistent with a high turnover of the actin filaments themselves. This explanation requires that a pool of αABD that dissociates from a filament due to actin depolymerization must have a higher probability of diffusing away than of rebinding to a neighboring actin filament.

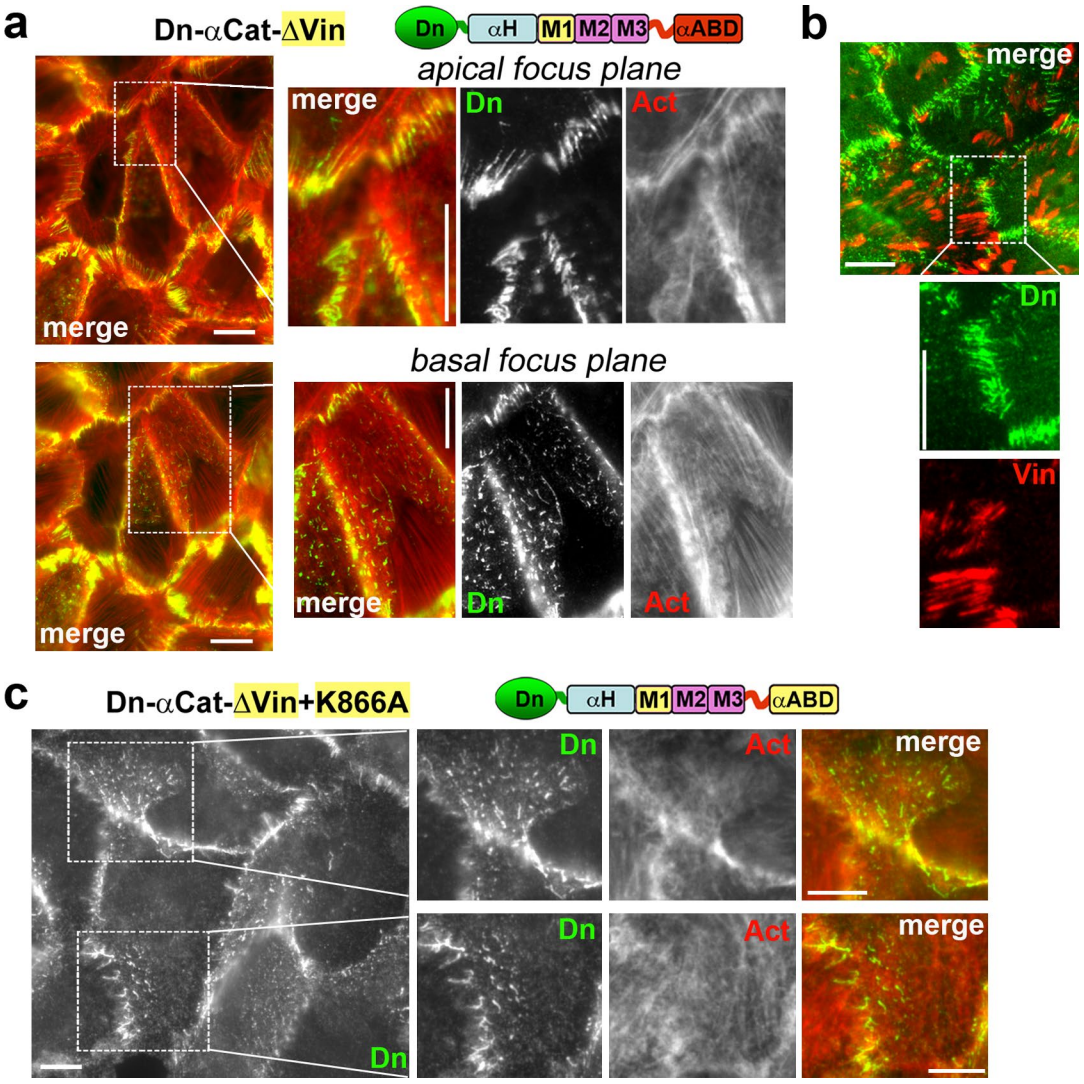

Figure 5. **AJs interact with actin filaments through αABD.** (a–c) Immunofluorescence microscopy of 468 cells expressing the α-catenin mutant, which interacts with actin specifically through αABD, Dn-αCat-ΔVin (a and b), or the same mutant with additional K866A point mutation (c). Cells were double stained for Dendra2 (Dn) and actin (Act; a) or Dn and vinculin (Vin; b). The boxed regions are magnified on the right. (a) The apical and basal focus planes are shown. Many apicolateral AJs of these cells were associated with the radial actin bundles. The cells were completely unable to produce basolateral AJs. (b) Vinculin is recruited only into the focal contacts. (c) 468 cells expressing Dn-αCat-ΔVin-K866A chimera have a phenotype similar to that of the parental cells (Fig. 3 a). Bars, 10 µm.

To verify the role of actin filament turnover in αABD dynamics, we globally blocked active intracellular processes by ATP depletion or specifically arrested actin dynamics by a triple-drug cocktail containing Jasplakinolide, Latrunculin B, and Y27632 (Peng et al., 2011). Both these approaches significantly slowed down dissipation of the red fluorescence in case of the intact protein but not of its K842A mutant (Fig. 9 b).

In a complementary approach, we photoconverted Dn-αABD at one part of the cell and tracked the photoconverted molecules in the nonconverted "dark" part of the same cell using high temporal resolution total internal reflection fluorescence (TIRF) microscopy. We expected that this imaging technique, known as fluorescent speckle microscopy (FSM; Danuser and Waterman-Storer, 2003), would reveal dynamics of the Dn-αABD clusters. Indeed, the photoconverted Dn-αABD was quickly recruited into the numerous speckles in the dark cell areas (Fig. 9, c and d; and Video 1). The modal lifespan of the speckle was ∼200–400 ms (Fig. 9 e), and new speckles were produced at the rate of 0.2 speckles/s/1 µm^2. The majority of the speckles showed virtually no displacement (Fig. 9 f). As expected, Dn-αABD, uncoupled from actin either by the point mutation I792A or by actin depolymerization by Latrunculin A, was unable to form the speckles (Figs. 8 and 9 c and Videos 2 and 3).

It is possible that each speckle originates from the fluorescence of a single Dn-αABD molecule. In this case, speckle dynamics represents a behavior of a single molecule in the cluster. Alternatively, a speckle could be formed as a result of simultaneous incorporation of many photoconverted molecules into the same cluster. In the latter case, speckle dynamics would reflect the dynamics of the αABD clusters. To distinguish between these possibilities, we fixed the cells 1 min after photoconversion, and the speckles formed around the photoconverted area were gradually photobleached with a 561-nm laser. Fig. 9 g shows that the speckle photobleaching kinetics were not stepwise, indicating that each speckle fluorescence was generated

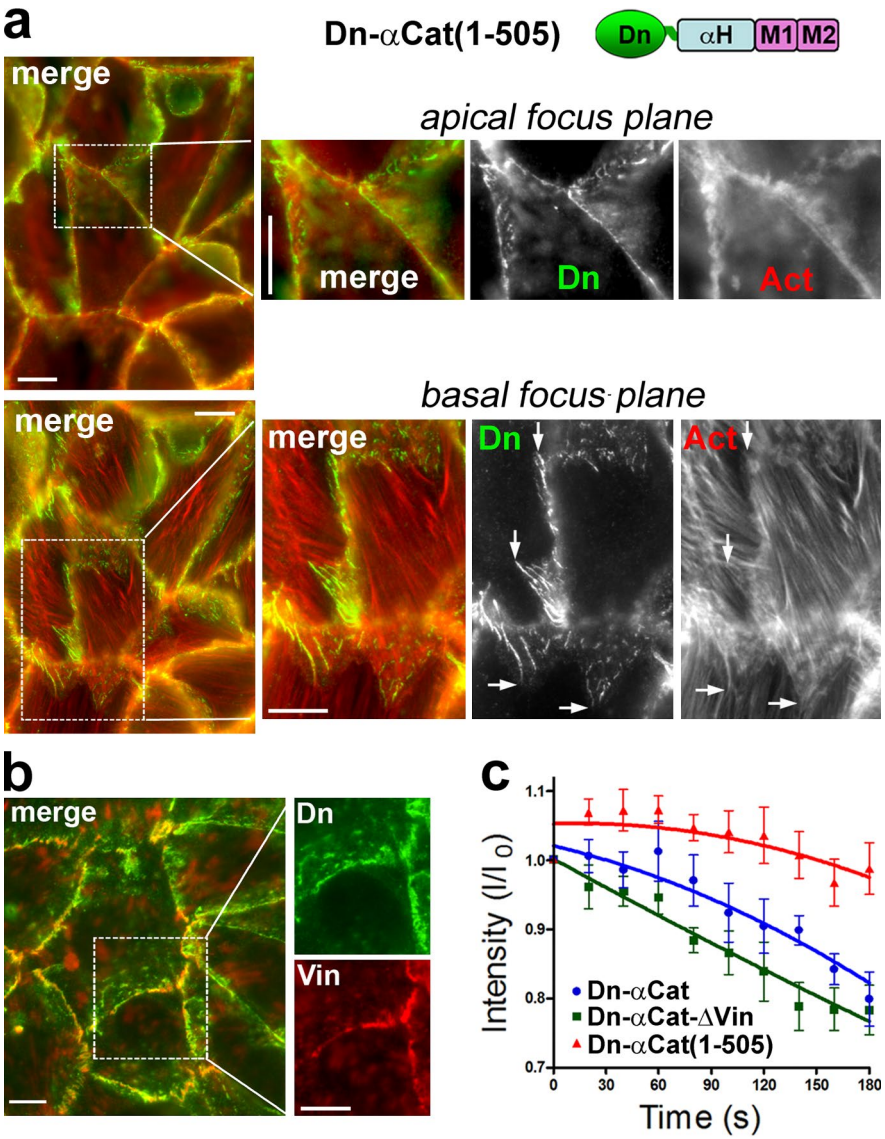

Figure 6. **AJs interacting with actin through vinculin produce static junctions.** (a and b) Immunofluorescence microscopy of 468 cells expressing the α-catenin deletion mutant, Dn-αCat(1–505). Cells were double stained for Dendra2 (Dn) and actin (Act; a) or Dn and vinculin (Vin; b). (a) Apicolateral AJs are associated with fine actin structures (apical focus plane). The basolateral junctions were also present but not associated with actin bundles (arrows, basal focus plane). (b) Apicolateral and lateral junctions both recruit vinculin. Bars, 10 µm. (c) Dendra photoconversion assay of the apicolateral AJs in 468 cells expressing Dn-αCat, Dn-αCat-ΔVin, or Dn-αCat(1–505). The intensity of the red fluorescence in the photoconverted spots decreases over time. The error bars represent SEs (n = 20).

by numerous molecules, thus favoring the second possibility—that speckle dynamics represent dynamics of the αABD clusters. Collectively, this live-imaging study shows that αABD clusters are continuously assembled and disassembled along the actin cortex with a fast turnover rate.

In the aforementioned experiments, we used isolated αABD. To validate that this domain is functional in full-length α-catenin, we expressed Dn-αCat and its mutant Dn-αCat-I792A in cadherin-deficient A431D cells at levels comparable to those of endogenous α-catenin (Fig. S5 a). Both proteins were cytosolic and their photoconverted fluorescence dissipated rapidly (Fig. S5 b). These observations suggested that Dn-αCat is a freely diffusing cytosolic protein in cadherin-deficient A431D cells. FSM, however, revealed that the Dn-αCat forms numerous speckles (Fig. S5, c and d), the mean lifetime of which was ∼400 ms shorter than speckle's lifetime of isolated αABD (Fig. S5 d, legend). Speckle formation was undetectable in cells expressing the Dn-αCat-I792A mutant. The predominant cytosolic localization of Dn-αCat in absence of cadherin and the short lifetime of its actin-bound clusters may be caused by differences in cooperativity between the binding of αABD and full-length α-catenin to actin filaments (Hansen et al., 2013).

We then studied whether αABD could cluster the cadherin–catenin complex. We constructed a Dendra-tagged tail domain of E-cadherin linked to the plasma membrane through a myristoylation signal (Ms-Dn-EcTail; Fig. S5), which is known to form a complex with the endogenous β- and α-catenins (Nieman et al., 1999). The Ms-Dn-EcTail was found to be concentrated in the areas enriched with cortical actin (Fig. S5 f), and FSM revealed the formation of numerous very sharp speckles. Latrunculin A abolished formation of such speckles, whereas some irregularities in the distribution of the Ms-Dn-EcTail remained (Fig. S5 g). It is possible that these irregularities, which were undetectable in the Latrunculin A–treated Dn-αABD– or Dn-αCat–expressing cells, were caused by some β-catenin–based interactions. Speckle stability was approximately the same as that of free α-catenin (compare Fig. S5, d and h). To show that speckle formation was driven by αABD, we expressed Ms-Dn-EcTail in cells in which α-catenin had been stably depleted by α-catenin–specific shRNA or in which α-catenin or its I792A mutant was reexpressed in the α-catenin–depleted cells. In agreement with the role of αABD in E-cadherin tail clustering, α-catenin–depleted cells as well as those expressing the I792A mutant exhibited the same pattern of Ms-

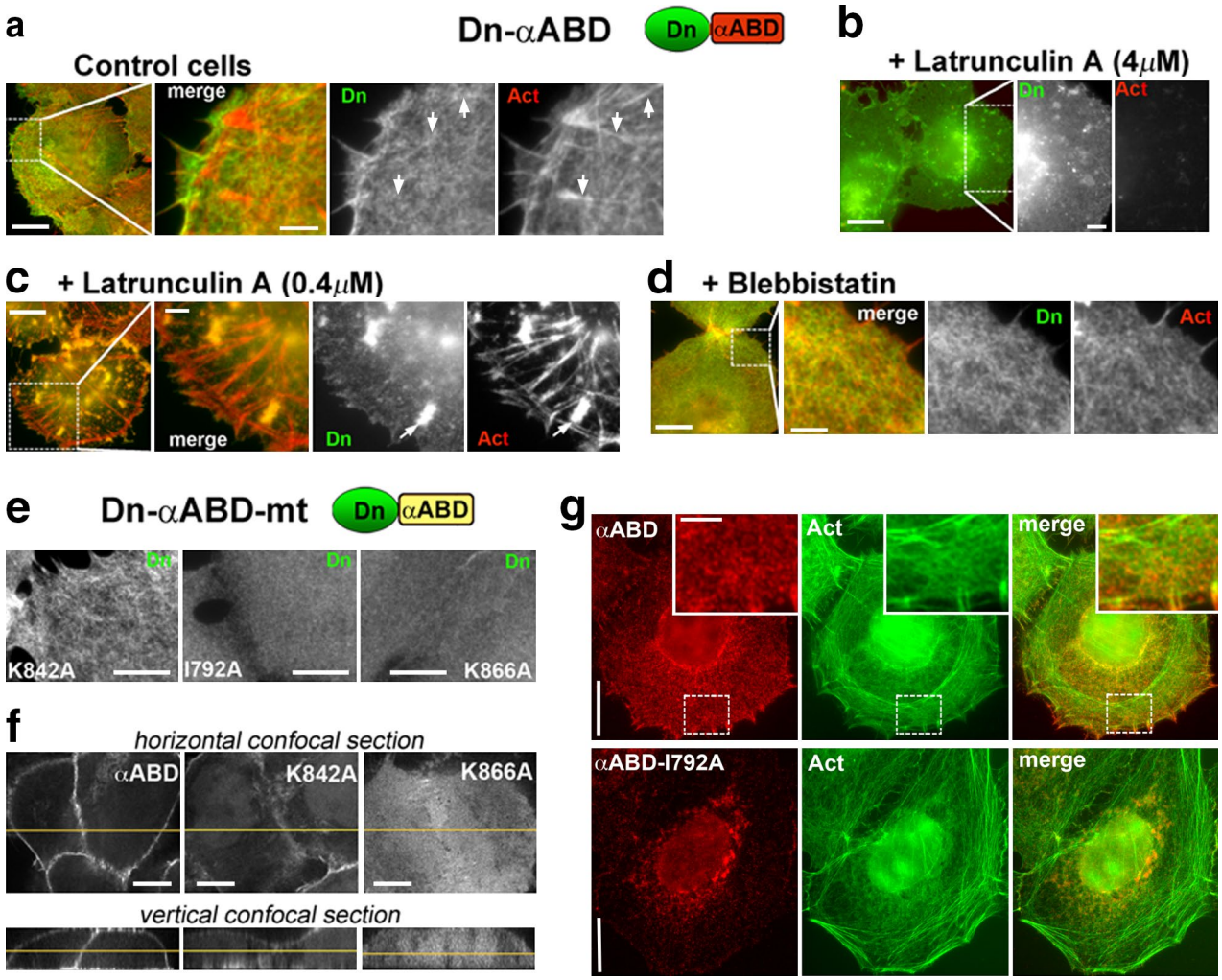

Figure 7. **Selective interaction of αABD with the actin cytoskeleton.** (a–d) Spatial localization of Dn-αABD (Dn, stained for Dendra2) and actin filaments (Act): (a) in A431 cells; (b) in A431 cells treated with a high dose of Latrunculin A for 10 min; (c) in A431 cells treated with a low dose of Latrunculin A for 10 min; and (d) in A431 cells treated with Blebbistatin for 15 min. The Dn-αABD chimera includes Dendra2 (Dn) and the 671–906 region of α-catenin (αABD). (e) Spatial localization of the Dn-αABD point mutants—K842A, I792A, and K866A—in A431 cells. (f) Confocal microscopy of A431 cells expressing Dn-αABD and its point mutants—K842A and K866A in horizontal and vertical cross sections (indicated by the yellow lines). (g) wt A431 cells were permeabilized with 0.025% saponin for 3 min and then incubated for another 5 min with His-mCherry–tagged αABD (αABD) or its inactive I792A version (αABD-I792A) and stained for actin. The boxed regions are magnified on the insets. Note that αABD preferentially decorates the cortex but shows very weak binding to the actin bundles. The I792A mutant shows only nonspecific binding. Arrows point to bundles (a) and cortical clumps (c). Bars: (main images) 10 μm; (magnified images) 2.5 μm.

Dn-EcTail distribution as control Ms-Dn-EcTail–expressing cells after Latrunculin A treatment (Fig. S5 g).

Discussion

The cadherin ectodomain alone can form junction-like structures through trans- and cis-intercadherin interactions (Wu et al., 2010; Hong et al., 2010, 2013; Harrison et al., 2011). These junctions, which likely resemble initial points of cell–cell attachment, are too dynamic and apparently too weak to maintain stable cell–cell adhesion unless they are reinforced by interactions with the actin cytoskeleton (Hong et al., 2013). As a step toward elucidating the interplay between intracellular, actin-binding, and extracellular, adhesive, processes in AJs, we sought to determine how α-catenin interacts with the actin cytoskeleton.

AJs can interact with the actin cytoskeleton using αABD

Although in vitro experiments have demonstrated that αABD binds directly to F-actin (Rimm et al., 1995; Pokutta et al., 2002; Pappas and Rimm, 2006), the role of this binding in vivo has been unclear. Indeed, αABD can also bind to actin indirectly through the actin-interacting proteins ZO1 and EPLIN (Imamura et al., 1999; Abe and Takeichi, 2008), whereas α-catenin in a cadherin–catenin complex in solution cannot bind actin (Drees et al., 2005; Yamada et al., 2005). Observations showing that αABD deletion attenuates AJ formation (Ozawa, 1998; Imamura et al., 1999; Yonemura et al., 2010; Twiss et al., 2012; Desai et al., 2013; Maiers et al., 2013; Thomas et al., 2013) could be interpreted to imply that deletion of αABD abolishes the binding of α-catenin with vinculin, EPLIN, or ZO1 by removing possible modes of indirect interactions.

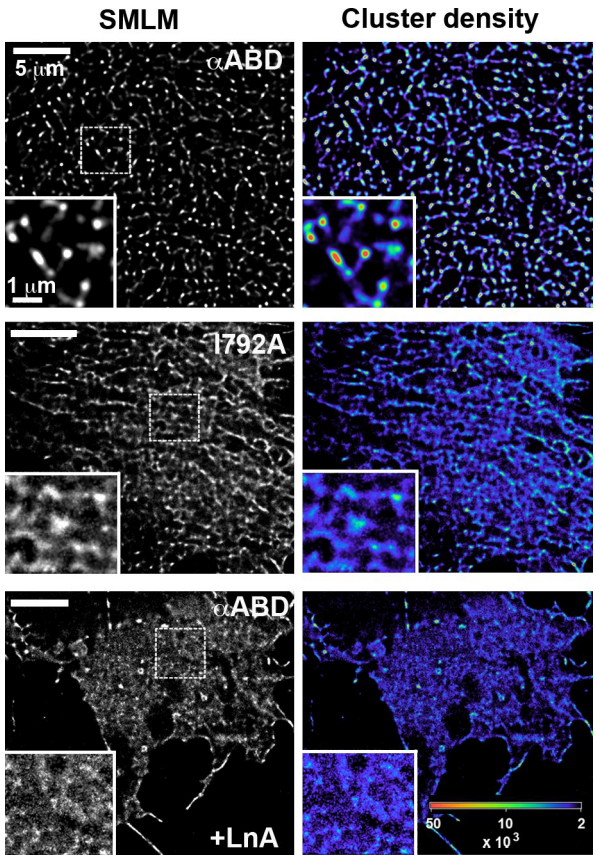

Figure 8. **SMLM of αABD clusters.** A431 cells expressing Dn-αABD (αABD), its point mutant Dn-αABD-I792A (I792A), or Dn-αABD after a 10-min treatment with Latrunculin A (LnA). The corresponding heat maps of molecular cluster densities are shown at the bottom with the heat bar given in the right corner. The boxed regions are magnified in the insets.

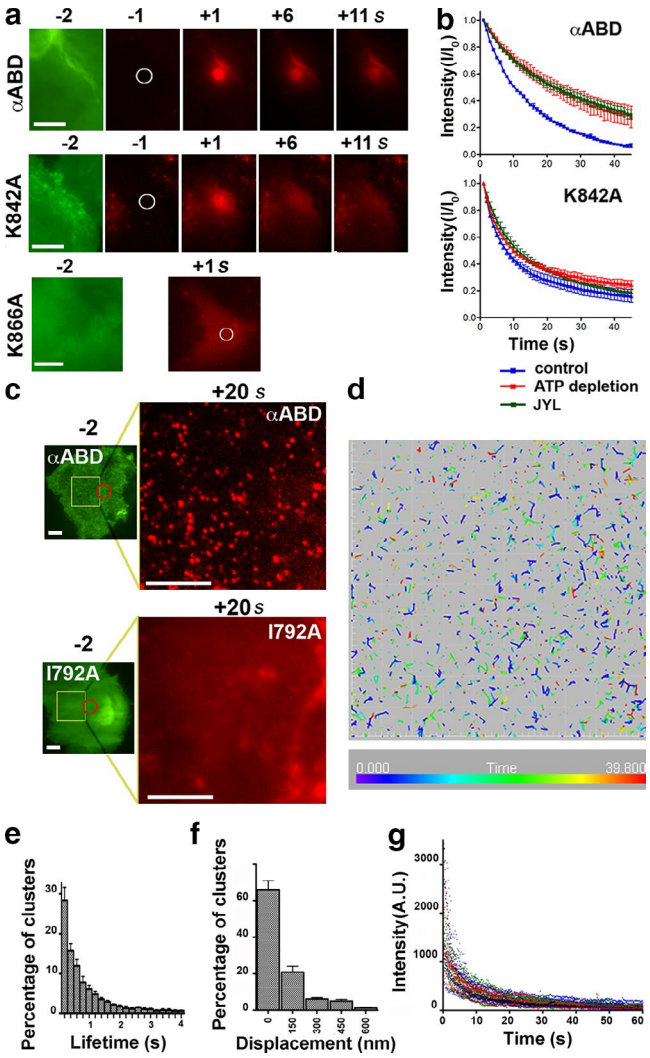

Figure 9. **Dynamic properties of αABD clusters.** (a) Dendra photoconversion assay of A431 cells expressing Dn-αABD (αABD) or its K842A or K866A point mutants. The images of green (−2) and red (−1) fluorescence were taken 2 and 1 s before photoconversion, respectively. The encircled areas (d = 2.5 µm) were converted from green to red fluorescence at time 0. After photoconversion, the red fluorescence was imaged in a stream mode with an image acquisition time of 1 s. Selected frames taken 1, 6, or 11 s after photoconversion (+1, +6, and +11) are shown. (b) Red fluorescence intensity over time in the photoconverted spots of A431 cells expressing Dn-αABD or its K842A point mutant. The curves were plotted based on experiments shown in Fig. 8 a (repeated 15 times) in unaffected A431 cells (control), in the cells with cytoskeleton stabilized by ATP depletion (ATP depletion), and in the cells with actin dynamics arrested by a triple-drug cocktail (JYL [Jasplakinolide, Latrunculin B, and Y27632]). Error bars indicate SEs. (c) FSM of A431 cells expressing Dn-αABD or its I792A point mutant. The encircled areas of the cells (d = ∼4 µm) were photoconverted to image the adjacent area (yellow boxes) for 40 s in a stream mode with 200-ms acquisition time (Videos 1 and 2, respectively). Frames taken 20 s after photoconversion (+20) are shown in the images on the right. (d) Spatial localization of αABD speckles plotted based on Video 1. The color of a given speckle corresponds to the moment of its appearance (the time bar is given at the bottom). (e) Lifetime distribution of αABD speckles. (f) Displacement of speckles (in nanometers) during their entire lifetime. Error bars in f and e indicate SDs. (g) The photobleaching curves of the individual speckles. A.U., arbitrary unit. Bars, 10 µm.

To clarify whether the in vivo interaction of αABD with actin in AJs is direct, indirect, or both, we exploited two new αABD point mutations, which dramatically decrease αABD actin-binding activity in vitro. These mutations were inserted into the chimeric protein EcΔ-Dn-α(280–906), which forms actin-associated AJ-like structures in A431D cadherin-deficient cells. No such structures were observed when the mutant chimeras were expressed. In contrast, the EcΔ-Dn-α(280–906)-ΔVin chimera, missing only the vinculin binding site, formed actin-associated junctions. ZO1 and EPLIN were also absent from these junctions. Together, these results strongly suggest that, in living cells, α-catenin can associate with actin through direct binding of αABD. However, these results, obtained using chimeric proteins, do not address the possibility that β-catenin–α-catenin interactions inhibit αABD in wt AJs.

To address this issue, we tested the α-catenin mutants in the context of full-length α-catenin transfected into α-catenin–deficient 468 cells. Consistent with results obtained with other vinculin-uncoupled α-catenin mutants (Huveneers et al., 2012; Twiss et al., 2012; Desai et al., 2013) and with vinculin-depleted cells (Watabe-Uchida et al., 1998; Taguchi et al., 2011), the α-catenin ΔVin mutant formed AJs, which, despite being devoid of vinculin, were still associated with an actin-enriched scaffold. Insertion of point mutations that inhibit αABD binding to actin completely abolished this association as well as AJ formation. Collectively, our results obtained using two cell models, A431D and 468 cells, strongly suggest that αABD directly links the cadherin–catenin complex to actin and that this interaction is sufficient for AJ assembly. This implies that the very

weak actin-binding activity of α-catenin in the cadherin–catenin complex detected in solution (Drees et al., 2005; Yamada et al., 2005) is enhanced in a cellular context. Whether this activation is based on force-dependent strengthening of αABD binding to actin (Buckley et al., 2014) and/or on cis-intercadherin interactions that could potentially support αABD–actin binding via a cooperative mechanism remains unclear.

A striking feature of the vinculin-deficient junctions is the very fast turnover of the α-catenin mutant Dn-αCat-ΔVin (Fig. 6 c). In this respect, these junctions are similar to AJs that incorporate wt α-catenin, which are also highly dynamic (Fig. 6 c). In contrast, the α-catenin mutant Dn-αCat(1–505), which assembles junctions through vinculin, is significantly less mobile. These findings suggest that the direct binding of αABD to the cytoskeleton is compatible with continuous reassembly of AJs, a process that has been previously reported (Adams et al., 1998; Yamada et al., 2005; Lambert et al., 2007; Cavey et al., 2008; de Beco et al., 2009; Canel et al., 2010; Hong et al., 2010). The fact that indirect, vinculin-based binding of α-catenin to actin is associated with much slower dynamics may suggest that vinculin, once it interacts with actin, suppresses AJ turnover. It is important to note that our staining for TJs (Fig. 4), as well as previous studies of force-dependent stabilization of AJs (Yonemura et al., 2010; Huveneers et al., 2012) or AJ-mediated adhesion strength (Thomas et al., 2013), suggested that neither αABD nor vinculin alone could produce fully functional AJs.

αABD forms transient actin-attached clusters

To understand how αABD binding to actin assembles AJs while also playing a role in AJ disassembly, we analyzed this binding in living cells. Our experiments reveal three previously unknown features of αABD–actin interactions. First, αABD binds exclusively to the actin cortex, a network of actin filaments attached to the inner face of the plasma membrane (Heuser and Kirschner, 1980; Svitkina et al., 2003; Morone et al., 2006). This observation suggests that AJs form their own actin bundles but do not interact with preexisting bundles, consistent with previous data showing the rapid reorganization of the actin cytoskeleton upon AJ formation (Adams et al., 1998; Vasioukhin et al., 2000; Mège et al., 2006). We speculate that some bundle-associated proteins, such as tropomyosin, might interfere with αABD binding either by masking binding sites along the filaments or by stabilizing a filament structure that is incompatible with αABD binding.

The second feature is that αABD, instead of being randomly bound to the cortex, exhibits a highly nonuniform distribution on actin filaments. This can be seen even with conventional immunofluorescence microscopy (Fig. 7 d), whereas superresolution SMLM shows the formation of discrete dense αABD clusters consisting of hundreds of molecules (Fig. 8). The formation of such clusters is consistent with in vitro experiments showing that αABD–actin binding is a highly cooperative process: actin filaments have a tendency to be either fully decorated by αABD or not decorated at all (Hansen et al., 2013), an observation that we have reproduced (unpublished data).

The third feature is that cortical αABD clusters are transient and dissociate in a time on the order of seconds (Fig. 9). Experiments with inhibitors of actin dynamics suggest that, at least in part, such short cluster lifetimes result from actin filament depolymerization. Consistently, a previous study found that the lifetime of individual actin filaments in a cell–cell contact area is ∼10 s (Yamada et al., 2005), whereas a more recent study suggested that a subpopulation of cortical filaments might have a lifetime significantly less than 5 s (Fritzsche et al., 2013).

Complementary roles of αABD and extracellular cadherin clusters in AJ assembly and dynamics

Each cell in a multicellular tissue must continuously readjust its AJs according to changes imposed by its own motility and by the motility of adjacent cells. At least in part, this AJ plasticity is mediated by the intrinsic flexibility of the AJ extracellular cadherin-mediated adhesive interface. This interface in vertebrate classical cadherins is mediated by a strand-swap trans-interaction and a cis-interaction, which together define an ordered structure that is similar for the type I cadherins (Harrison et al., 2011). The trans-adhesive interface exhibits fast rebinding kinetics as a result of binding intermediates called X-dimers (Harrison et al., 2010; Hong et al., 2011). Structural (Harrison et al., 2011), computational (Wu et al., 2010), cell biological (Hong et al., 2013; Strale et al., 2015), and biochemical (Klingelhöfer et al., 2002; Troyanovsky et al., 2006, 2007) studies suggest that the AJ adhesive interface in vertebrates is organized in numerous small adhesive clusters, whose individual instability and fast reassembly maintain both integrity and flexibility of the cell–cell interface.

Interactions between cadherin and the cytoskeleton, however, also appear to be unstable, allowing cadherin molecules to move in and out of AJs, with the lifetime of a cadherin molecule bound in an AJ estimated at less than a minute (de Beco et al., 2009; Hong et al., 2010). Our observation that αABD forms transient actin cortex-bound clusters (Figs. 8 and 9) suggests a source for this instability. Furthermore, it shows that both the adhesive interface and the actin-binding interface of AJs consist of numerous reassembling clusters. This concordance implies that the two types of clusters are functionally interconnected. Experimental observations on basal-to-apical flow of cadherin clusters also support this suggestion (Kametani and Takeichi, 2007). This work observed that basal–apical flow was disrupted upon αABD deletion, indicating that movement of cadherin clusters depends on αABD–actin clustering. Interestingly, although fluorescent speckle microscopy showed that αABD is able to cluster full-length α-catenin as well as the myristoylated E-cadherin tail (Fig. S5), we were unable to detect clustering of full-length E-cadherin (unpublished data). This may be caused by slow E-cadherin diffusion and a low concentration of this protein at the ventral membrane.

A plausible hypothesis for the mechanism of cadherin–αABD interplay is that a build-up of cadherins in cell–cell contact regions as a result of a diffusion trap mechanism and the subsequent formation of small ordered clusters involving trans- and cis-interactions between cadherin ectodomains, nucleates formation of αABD-based clusters inside the cell. The αABD-based clusters could, in turn, reinforce the intercadherin interactions in the ectodomain clusters, thereby enhancing their adhesive function. The resulting cadherin/αABD-based clusters—transient, as a result of actin depolymerization, and highly adhesive, as a result of anchorage to cortical actin filaments—could provide a partial basis for AJ plasticity. In this way, both the intracellular and extracellular regions of cadherins could collaborate to maximize cadherin concentration at intercellular junctions and to enhance the general stability of the junctions.

Although additional studies are required to firmly establish this hypothesis, an interplay between these two types of clustering mechanisms would explain the highly dynamic nature of the αABD-only junctions (Fig. 6 c), the ATP dependence of cadherin turnover in AJs (Troyanovsky et al., 2006), and why polymerization of new actin filaments is required for AJ integrity (Vasioukhin et al., 2000; Zhang et al., 2005).

Materials and methods

Plasmids

The plasmids (all in pRcCMV; Invitrogen) encoding chimeric protein EcΔ-Dn-α(280–906) presented in Fig. 2 were based on EcΔDn (Hong et al., 2010). The general maps of the EcΔ-Dn-α(280–906) chimera, Dn-α-catenin, Dn-αABD, and their mutants (also in pRcCMV) are presented in Figs. 2, 3, 4, and 5. The α-catenin mutation inactivating its vinculin binding site was constructed based on the structural studies (Choi et al., 2012; Rangarajan and Izard, 2012). It includes five amino acid substitutions to alanine: R329A, R330A, L347A, L348A, and Y351A. The shRNA-target region of α-catenin (5′-CCTGTTCCATCTCAAATAA-3′) in the plasmids used in α-catenin–silenced A431 cells was modified using PCR-directed mutagenesis. The original plasmid encoding human αE-catenin was published (Troyanovsky et al., 2011). All plasmid inserts were verified by sequencing.

Cell culture and transfection

Transfection and growth of A431D (provided by J.K. Wahl, The University of Nebraska, Lincoln, NE), A431, and 468 cells were performed as previously described (Troyanovsky et al., 2011). After antibiotic selection, the cells were sorted for moderate transgene expression by FACS. Lentiviral knockdown (shRNA) plasmids (V2LHS-262377; GE Healthcare) were obtained from C. Gottardi and A. Yemelyanov (Northwestern University, Chicago, IL). Before use, the GFP-encoding region of this plasmid was deleted. The infected cells were selected with 5 µg/ml puromycin.

Immunofluorescence microscopy

For immunofluorescence, cells were fixed and permeabilized either with methanol-acetone or, in case of phalloidin staining, with 3% formaldehyde–1% Triton X-100, or, in case of anti-vinculin staining, with BM[PEO]3 (see Indra et al., 2013 for details). Wide-field images were taken using a microscope (Plan Apochromat 100×/1.40 NA objective lens; Eclipse 80i; Nikon) and a digital camera (CoolSNAP EZ; Photometrics). The images were then processed using NIS-Elements software (Nikon). The following antibodies were used: mouse anti–E-cadherin and anti-occludin (Invitrogen), rabbit anti-Dendra2 (Evrogen), mouse anti–β-catenin and ZO1 (BD), mouse anti-vinculin and rabbit anti-EPLIN (Sigma-Aldrich), goat anti–α-catenin (Santa Cruz Biotechnology, Inc.), rabbit anti–α-catenin N-terminal domain, EP1993Y (Abcam), and guinea pig anti-cingulin (provided by I. Hofmann, German Cancer Research Center, Heidelberg, Germany). Alexa Fluor 555 phalloidin and Latrunculin A were purchased from Invitrogen.

Live-cell imaging and data processing

These experiments were performed essentially as described previously (Hong et al., 2010, 2013). In brief, cells were imaged (in L-15 plus 10% FBS) by a microscope (Eclipse Ti-E; Nikon) at 37°C controlled with NIS-Elements software. The microscope was equipped with an incubator chamber, a camera (CoolSNAP HQ2; Photometrics), Plan Apochromat 60×/1.40 NA and Plan Apochromat VC 100×/1.40 NA lenses, and halogen and mercury light sources. Time-lapse images were taken in both FITC and mCherry filter sets using halogen light that minimized phototoxicity and photobleaching. To analyze cadherin junctional turnover, we used a junctional Dendra photoconversion assay (Hong et al., 2013) in which the point of interest (φ = 2.5 µm) was photoconverted by a 100-ms-long exposure to the 402-nm wavelength laser. Time-lapse images were then taken in a red channel in a stream mode with 1 s (in Fig. 7 h) or in 20-s intervals with 1 s (Fig. 6 c) of image acquisition time. In some cases, the cells immediately before photoconversion were cultured for 5 min in ATP depletion media (Hong et al., 2010).

All images were saved as TIFF files and processed using ImageJ software (National Institutes of Health). In the Dendra photoconversion assay, the red fluorescent intensity was normalized in such a way that 0 and 1 corresponded to the background and the initial (immediately after activation) values. The background value was obtained from the image taken right before the photoconversion. The time course of the intensity change was produced from 10 sets of independent experiments. Mean values were calculated for each time point.

For SMLM, the cells were cultured on glass-bottom dish (P35G-1.5; MatTek Corporation) overnight and then fixed with 3% paraformaldehyde and 0.1% glutaraldehyde for 10 min at room temperature. After washing three times, the cells were immersed in the freshly prepared image buffer containing 50 mM Tris-HCl, pH 8.0, 10 mM NaCl, 10% glucose, 5 mg/ml glucose oxidase, 0.4 µg/ml catalase, and 0.1 M β-mercaptoethylamine. Samples were sealed immediately after adding image buffer. The N-STORM system (Nikon) with a camera (DU897; Andor Technology) was used for superresolution image acquisition. 20,000–40,000 images were acquired at 29-ms/frame exposure time via TIRF illumination, using a Plan Apochromatic TIRF 100× 1.49 NA objective lens. Dendra-fused proteins were activated with a 405-nm laser and acquired with 561-nm laser illumination. The images were rendered using the built-in N-STORM single molecule localization analysis algorithms.

For the spinning-disk confocal microscopy and FSM, the inverted microscope (Nikon-Ti) equipped with a TIRF illuminator module (Nikon) and spinning-disk unit (CSU-X1; Yokogawa Electric Corporation) was used. The cells were imaged in CO_2 stage incubator (37°C) during all live-cell imaging process. To identify the spatial distribution of Dn-αABD and its mutants, 0.3-µm-thick optical sections were taken through whole cells using confocal mode with 488-nm illumination. Optical sections were acquired using NIS-Elements software. For FSM, Dn-tagged molecules were photoconverted using a 405-nm laser within the area of ∼4 µm in diameter, and the converted molecules were imaged for 40 s in the adjacent nonphotoconverted area (20×20 µm^2) using the 561-nm laser illumination (30% of intensity was used to minimize photobleaching). Images were acquired using TIRF microscopy with Plan Apochromatic TIRF 100×, 1.49 NA objective lens and camera (iXon3; Andor Technology) at 5 Hz frame rate. The spatial and temporal positions of the clusters were analyzed using Imaris 7.3 (Bitplane). Background subtraction and fluorescent speckle selection were performed with Imaris built-in algorithms. Image stacks were recorded for each protein ($n > 5$), and >1,000 speckles were tracked in each image stack. For the cluster photobleach experiment (Fig. 8 f), the cells were fixed with 3% paraformaldehyde on a microscope stage 1 min after photoconversion. Time series images were acquired under same condition as FSM but with 60% 561-nm laser intensity to photobleach αABD clusters.

Actin cosedimentation and αABD-incorporation assays

For recombinant GST fusion protein production, the indicated α-catenin DNA fragments were subcloned into the bacterial expression vector pGEX-4T-1, which places GST in front of the αABD. The resulting plasmids were transformed into BL21(DE3) cells. Protein purifica-

tion was performed using GST SpinTrap columns with no deviation from the manufacturer's protocol (GE Healthcare). The cosedimentation assay and determination of binding affinities were performed according to the published protocol (Pappas and Rimm, 2006). In brief, the prepolymerized actin filaments (rabbit skeletal muscle actin was purchased from the Cytoskeleton, Inc.) in F buffer (2 mM Tris, pH 8.0, 50 mM KCl, 2 mM $MgCl_2$, 1 mM ATP, 1 mM EGTA, and 1 mM DTT) were incubated with precleared (100,000 *g* for 30 min) recombinant proteins for 30 min at room temperature. The preclearing step completely removed nonspecific sedimentation of the recombinant proteins in the absence of actin. The reaction was centrifuged at 100,000 *g* for 30 min. Equivalent volumes of pellet and supernatant fractions were analyzed by SDS-PAGE and densitometry. To assess binding affinities, three independent experiments each of which included αABD and three its mutants were performed, one of which is shown in Fig. 1 e. Although binding curves for the mutants varied between the experiments, the K842A mutant always exhibited slightly better binding than other mutants.

To test αABD binding with specific actin filament structures (Fig. 7 g), subconfluent cultures of A431 cells were first incubated for 3 min in permeabilization buffer (140 mM KCl, 10 mM Hepes, pH 7.0, 3 mM EGTA, 4 mM $MgCl_2$, 1% BSA, and 0.05% saponin) and then for 5 min in the same buffer with 1.2 µg/ml of the recombinant polyhistidine/mCherry-tagged αABD. Cells then were briefly washed in the same buffer, fixed, and processed for anti-actin staining.

Online supplemental material

Fig. S1 shows multiple structure-based sequence alignment of orthologous actin binding domains of α-catenin and vinculin. Fig. S2 shows junctions made of the EcΔ-Dn-α(280–906)-ΔVin chimera in A431D cells are devoid of the actin-binding proteins ZO1 and EPLIN. Fig. S3 shows AJs of α-catenin–deficient 468 cells and the same cells expressing the Dn-αCat-ΔVin mutant. Fig. S4 shows Western blotting assays using the anti–α-catenin antibody (EP1993Y) to probe expression levels of Dn-αCat and its mutants. Fig. S5 shows dynamic properties of clusters formed by the full-length α-catenin and myristoylated E-cadherin tail. Video 1 shows FSM of Dn-αABD clusters in A431 cells. Video 2 shows FSM of Dn-αABD in Latrunculin A–treated A431 cells. Video 3 shows FSM of Dn-αABD-I792A mutant in A431 cells. Online supplemental material is available at http://www.jcb.org/cgi/content/full/jcb.201412064/DC1.

Acknowledgments

We are grateful to Dr. I. Hofmann (German Cancer Research Center), Dr. J.K. Wahl (The University of Nebraska Medical Center, Lincoln, NE), and Drs. C. Gottardi and A. Yemelyanov (Feinberg School of Medicine, Northwestern University, Chicago, IL) for providing the anti-cingulin antibody, A431D cells, and α-catenin shRNA lentivirus, correspondingly. Sequencing, flow cytometry, and SMLM were performed at the Northwestern University Genetic, Flow Cytometry, and Advanced Microscopy Centers.

The work was supported by grants from the National Institutes of Health, AR44016 and AR057992 (to S.M. Troyanovsky) and GM062270 (to L. Shapiro), and a grant from a National Science Foundation, MCB-1412472 (to B. Honig).

The authors declare no competing financial interests.

Submitted: 12 December 2014
Accepted: 13 July 2015

References

Abe, K., and M. Takeichi. 2008. EPLIN mediates linkage of the cadherin catenin complex to F-actin and stabilizes the circumferential actin belt. *Proc. Natl. Acad. Sci. USA.* 105:13–19. http://dx.doi.org/10.1073/pnas.0710504105

Adams, C.L., and W.J. Nelson. 1998. Cytomechanics of cadherin-mediated cell-cell adhesion. *Curr. Opin. Cell Biol.* 10:572–577. http://dx.doi.org/10.1016/S0955-0674(98)80031-8

Adams, C.L., Y.T. Chen, S.J. Smith, and W.J. Nelson. 1998. Mechanisms of epithelial cell–cell adhesion and cell compaction revealed by high-resolution tracking of E-cadherin–green fluorescent protein. *J. Cell Biol.* 142:1105–1119. http://dx.doi.org/10.1083/jcb.142.4.1105

Brasch, J., O.J. Harrison, B. Honig, and L. Shapiro. 2012. Thinking outside the cell: how cadherins drive adhesion. *Trends Cell Biol.* 22:299–310. http://dx.doi.org/10.1016/j.tcb.2012.03.004

Buckley, C.D., J. Tan, K.L. Anderson, D. Hanein, N. Volkmann, W.I. Weis, W.J. Nelson, and A.R. Dunn. 2014. Cell adhesion. The minimal cadherin-catenin complex binds to actin filaments under force. *Science.* 346:1254211. http://dx.doi.org/10.1126/science.1254211

Canel, M., A. Serrels, K.I. Anderson, M.C. Frame, and V.G. Brunton. 2010. Use of photoactivation and photobleaching to monitor the dynamic regulation of E-cadherin at the plasma membrane. *Cell Adhes. Migr.* 4:491–501. http://dx.doi.org/10.4161/cam.4.4.12661

Cavey, M., M. Rauzi, P.F. Lenne, and T. Lecuit. 2008. A two-tiered mechanism for stabilization and immobilization of E-cadherin. *Nature.* 453:751–756. http://dx.doi.org/10.1038/nature06953

Choi, H.J., S. Pokutta, G.W. Cadwell, A.A. Bobkov, L.A. Bankston, R.C. Liddington, and W.I. Weis. 2012. αE-catenin is an autoinhibited molecule that coactivates vinculin. *Proc. Natl. Acad. Sci. USA.* 109:8576–8581. http://dx.doi.org/10.1073/pnas.1203906109

Danuser, G., and C.M. Waterman-Storer. 2003. Quantitative fluorescent speckle microscopy: where it came from and where it is going. *J. Microsc.* 211:191–207. http://dx.doi.org/10.1046/j.1365-2818.2003.01222.x

de Beco, S., C. Gueudry, F. Amblard, and S. Coscoy. 2009. Endocytosis is required for E-cadherin redistribution at mature adherens junctions. *Proc. Natl. Acad. Sci. USA.* 106:7010–7015. http://dx.doi.org/10.1073/pnas.0811253106

Desai, R., R. Sarpal, N. Ishiyama, M. Pellikka, M. Ikura, and U. Tepass. 2013. Monomeric α-catenin links cadherin to the actin cytoskeleton. *Nat. Cell Biol.* 15:261–273. http://dx.doi.org/10.1038/ncb2685

Drees, F., S. Pokutta, S. Yamada, W.J. Nelson, and W.I. Weis. 2005. α-catenin is a molecular switch that binds E-cadherin-β-catenin and regulates actin-filament assembly. *Cell.* 123:903–915. http://dx.doi.org/10.1016/j.cell.2005.09.021

Fritzsche, M., A. Lewalle, T. Duke, K. Kruse, and G. Charras. 2013. Analysis of turnover dynamics of the submembranous actin cortex. *Mol. Biol. Cell.* 24:757–767. http://dx.doi.org/10.1091/mbc.E12-06-0485

Gomez, G.A., R.W. McLachlan, and A.S. Yap. 2011. Productive tension: force-sensing and homeostasis of cell-cell junctions. *Trends Cell Biol.* 21:499–505. http://dx.doi.org/10.1016/j.tcb.2011.05.006

Green, K.J., S. Getsios, S. Troyanovsky, and L.M. Godsel. 2010. Intercellular junction assembly, dynamics, and homeostasis. *Cold Spring Harb. Perspect. Biol.* 2:a000125. http://dx.doi.org/10.1101/cshperspect.a000125

Gumbiner, B.M. 2005. Regulation of cadherin-mediated adhesion in morphogenesis. *Nat. Rev. Mol. Cell Biol.* 6:622–634. http://dx.doi.org/10.1038/nrm1699

Hansen, S.D., A.V. Kwiatkowski, C.Y. Ouyang, H. Liu, S. Pokutta, S.C. Watkins, N. Volkmann, D. Hanein, W.I. Weis, R.D. Mullins, and W.J. Nelson. 2013. αE-catenin actin-binding domain alters actin filament conformation and regulates binding of nucleation and disassembly factors. *Mol. Biol. Cell.* 24:3710–3720. http://dx.doi.org/10.1091/mbc.E13-07-0388

Harrison, O.J., F. Bahna, P.S. Katsamba, X. Jin, J. Brasch, J. Vendome, G. Ahlsen, K.J. Carroll, S.R. Price, B. Honig, and L. Shapiro. 2010. Two-step adhesive binding by classical cadherins. *Nat. Struct. Mol. Biol.* 17:348–357. http://dx.doi.org/10.1038/nsmb.1784

Harrison, O.J., X. Jin, S. Hong, F. Bahna, G. Ahlsen, J. Brasch, Y. Wu, J. Vendome, K. Felsovalyi, C.M. Hampton, et al. 2011. The extracellular architecture of adherens junctions revealed by crystal structures of type I cadherins. *Structure.* 19:244–256. http://dx.doi.org/10.1016/j.str.2010.11.016

Hazan, R.B., L. Kang, S. Roe, P.I. Borgen, and D.L. Rimm. 1997. Vinculin is associated with the E-cadherin adhesion complex. *J. Biol. Chem.* 272:32448–32453. http://dx.doi.org/10.1074/jbc.272.51.32448

Heuser, J.E., and M.W. Kirschner. 1980. Filament organization revealed in platinum replicas of freeze-dried cytoskeletons. *J. Cell Biol.* 86:212–234. http://dx.doi.org/10.1083/jcb.86.1.212

Hong, S., R.B. Troyanovsky, and S.M. Troyanovsky. 2010. Spontaneous assembly and active disassembly balance adherens junction homeostasis. *Proc. Natl. Acad. Sci. USA.* 107:3528–3533. http://dx.doi.org/10.1073/pnas.0911027107

Hong, S., R.B. Troyanovsky, and S.M. Troyanovsky. 2011. Cadherin exits the junction by switching its adhesive bond. *J. Cell Biol.* 192:1073–1083. http://dx.doi.org/10.1083/jcb.201006113

Hong, S., R.B. Troyanovsky, and S.M. Troyanovsky. 2013. Binding to F-actin guides cadherin cluster assembly, stability, and movement. *J. Cell Biol.* 201:131–143. http://dx.doi.org/10.1083/jcb.201211054

Huveneers, S., J. Oldenburg, E. Spanjaard, G. van der Krogt, I. Grigoriev, A. Akhmanova, H. Rehmann, and J. de Rooij. 2012. Vinculin associates with endothelial VE-cadherin junctions to control force-dependent remodeling. *J. Cell Biol.* 196:641–652. http://dx.doi.org/10.1083/jcb.201108120

Imamura, Y., M. Itoh, Y. Maeno, S. Tsukita, and A. Nagafuchi. 1999. Functional domains of α-catenin required for the strong state of cadherin-based cell adhesion. *J. Cell Biol.* 144:1311–1322. http://dx.doi.org/10.1083/jcb.144.6.1311

Indra, I., S. Hong, R. Troyanovsky, B. Kormos, and S. Troyanovsky. 2013. The adherens junction: a mosaic of cadherin and nectin clusters bundled by actin filaments. *J. Invest. Dermatol.* 133:2546–2554. http://dx.doi.org/10.1038/jid.2013.200

Ishiyama, N., N. Tanaka, K. Abe, Y.J. Yang, Y.M. Abbas, M. Umitsu, B. Nagar, S.A. Bueler, J.L. Rubinstein, M. Takeichi, and M. Ikura. 2013. An autoinhibited structure of α-catenin and its implications for vinculin recruitment to adherens junctions. *J. Biol. Chem.* 288:15913–15925. http://dx.doi.org/10.1074/jbc.M113.453928

Ivanov, A.I., and N.G. Naydenov. 2013. Dynamics and regulation of epithelial adherens junctions: recent discoveries and controversies. *Int Rev Cell Mol Biol.* 303:27–99. http://dx.doi.org/10.1016/B978-0-12-407697-6.00002-7

Kametani, Y., and M. Takeichi. 2007. Basal-to-apical cadherin flow at cell junctions. *Nat. Cell Biol.* 9:92–98. http://dx.doi.org/10.1038/ncb1520

Klingelhöfer, J., O.Y. Laur, R.B. Troyanovsky, and S.M. Troyanovsky. 2002. Dynamic interplay between adhesive and lateral E-cadherin dimers. *Mol. Cell. Biol.* 22:7449–7458. http://dx.doi.org/10.1128/MCB.22.21.7449-7458.2002

Kobielak, A., and E. Fuchs. 2004. α-catenin: at the junction of intercellular adhesion and actin dynamics. *Nat. Rev. Mol. Cell Biol.* 5:614–625. http://dx.doi.org/10.1038/nrm1433

Kusumi, A., K. Suzuki, and K. Koyasako. 1999. Mobility and cytoskeletal interactions of cell adhesion receptors. *Curr. Opin. Cell Biol.* 11:582–590. http://dx.doi.org/10.1016/S0955-0674(99)00020-4

Lambert, M., O. Thoumine, J. Brevier, D. Choquet, D. Riveline, and R.M. Mège. 2007. Nucleation and growth of cadherin adhesions. *Exp. Cell Res.* 313:4025–4040. http://dx.doi.org/10.1016/j.yexcr.2007.07.035

Maiers, J.L., X. Peng, A.S. Fanning, and K.A. DeMali. 2013. ZO-1 recruitment to α-catenin—a novel mechanism for coupling the assembly of tight junctions to adherens junctions. *J. Cell Sci.* 126:3904–3915. http://dx.doi.org/10.1242/jcs.126565

Mège, R.M., J. Gavard, and M. Lambert. 2006. Regulation of cell-cell junctions by the cytoskeleton. *Curr. Opin. Cell Biol.* 18:541–548. http://dx.doi.org/10.1016/j.ceb.2006.08.004

Morone, N., T. Fujiwara, K. Murase, R.S. Kasai, H. Ike, S. Yuasa, J. Usukura, and A. Kusumi. 2006. Three-dimensional reconstruction of the membrane skeleton at the plasma membrane interface by electron tomography. *J. Cell Biol.* 174:851–862. http://dx.doi.org/10.1083/jcb.200606007

Nagafuchi, A., S. Ishihara, and S. Tsukita. 1994. The roles of catenins in the cadherin-mediated cell adhesion: functional analysis of E-cadherin-α catenin fusion molecules. *J. Cell Biol.* 127:235–245. http://dx.doi.org/10.1083/jcb.127.1.235

Nieman, M.T., J.B. Kim, K.R. Johnson, and M.J. Wheelock. 1999. Mechanism of extracellular domain-deleted dominant negative cadherins. *J. Cell Sci.* 112:1621–1632.

Niessen, C.M., D. Leckband, and A.S. Yap. 2011. Tissue organization by cadherin adhesion molecules: dynamic molecular and cellular mechanisms of morphogenetic regulation. *Physiol. Rev.* 91:691–731. http://dx.doi.org/10.1152/physrev.00004.2010

Ozawa, M. 1998. Identification of the region of α-catenin that plays an essential role in cadherin-mediated cell adhesion. *J. Biol. Chem.* 273:29524–29529. http://dx.doi.org/10.1074/jbc.273.45.29524

Pappas, D.J., and D.L. Rimm. 2006. Direct interaction of the C-terminal domain of alpha-catenin and F-actin is necessary for stabilized cell-cell adhesion. *Cell Commun. Adhes.* 13:151–170. http://dx.doi.org/10.1080/15419060600726142

Peng, X., L.E. Cuff, C.D. Lawton, and K.A. DeMali. 2010. Vinculin regulates cell-surface E-cadherin expression by binding to beta-catenin. *J. Cell Sci.* 123:567–577. http://dx.doi.org/10.1242/jcs.056432

Peng, G.E., S.R. Wilson, and O.D.A. Weiner. 2011. A pharmacological cocktail for arresting actin dynamics in living cells. *Mol. Biol. Cell.* 22:3986–3994. http://dx.doi.org/10.1091/mbc.E11-04-0379

Pokutta, S., F. Drees, Y. Takai, W.J. Nelson, and W.I. Weis. 2002. Biochemical and structural definition of the l-afadin- and actin-binding sites of α-catenin. *J. Biol. Chem.* 277:18868–18874. http://dx.doi.org/10.1074/jbc.M201463200

Rangarajan, E.S., and T. Izard. 2012. The cytoskeletal protein α-catenin unfurls upon binding to vinculin. *J. Biol. Chem.* 287:18492–18499. http://dx.doi.org/10.1074/jbc.M112.351023

Rangarajan, E.S., and T. Izard. 2013. Dimer asymmetry defines α-catenin interactions. *Nat. Struct. Mol. Biol.* 20:188–193. http://dx.doi.org/10.1038/nsmb.2479

Ray, S., H.P. Foote, and T. Lechler. 2013. β-Catenin protects the epidermis from mechanical stresses. *J. Cell Biol.* 202:45–52.

Rimm, D.L., E.R. Koslov, P. Kebriaei, C.D. Cianci, and J.S. Morrow. 1995. α1(E)-catenin is an actin-binding and -bundling protein mediating the attachment of F-actin to the membrane adhesion complex. *Proc. Natl. Acad. Sci. USA.* 92:8813–8817. http://dx.doi.org/10.1073/pnas.92.19.8813

Strale, P.O., L.Duchesne, G.Peyret, L.Montel, T.Nguyen, E.Png, R.Tampé, S.Troyanovsky, S.Hénon, B.Ladoux, and R.M.Mège. 2015. The formation of ordered nanoclusters controls cadherin anchoring to actin and cell-cell contact fluidity. *J. Cell Biol.*210:333–346. http://dx.doi.org/10.1083/jcb.201410111

Svitkina, T.M., E.A. Bulanova, O.Y. Chaga, D.M. Vignjevic, S. Kojima, J.M. Vasiliev, and G.G. Borisy. 2003. Mechanism of filopodia initiation by reorganization of a dendritic network. *J. Cell Biol.* 160:409–421. http://dx.doi.org/10.1083/jcb.200210174

Taguchi, K., T. Ishiuchi, and M. Takeichi. 2011. Mechanosensitive EPLIN-dependent remodeling of adherens junctions regulates epithelial reshaping. *J. Cell Biol.* 194:643–656. http://dx.doi.org/10.1083/jcb.201104124

Takeichi, M. 2014. Dynamic contacts: rearranging adherens junctions to drive epithelial remodelling. *Nat. Rev. Mol. Cell Biol.* 15:397–410. http://dx.doi.org/10.1038/nrm3802

Thievessen, I., P.M. Thompson, S. Berlemont, K.M. Plevock, S.V. Plotnikov, A. Zemljic-Harpf, R.S. Ross, M.W. Davidson, G. Danuser, S.L. Campbell, and C.M. Waterman. 2013. Vinculin-actin interaction couples actin retrograde flow to focal adhesions, but is dispensable for focal adhesion growth. *J. Cell Biol.* 202:163–177. http://dx.doi.org/10.1083/jcb.201303129

Thomas, W.A., C. Boscher, Y.S. Chu, D. Cuvelier, C. Martinez-Rico, R. Seddiki, J. Heysch, B. Ladoux, J.P. Thiery, R.M. Mege, and S. Dufour. 2013. α-Catenin and vinculin cooperate to promote high E-cadherin-based adhesion strength. *J. Biol. Chem.* 288:4957–4969. http://dx.doi.org/10.1074/jbc.M112.403774

Thompson, P.M., C.E. Tolbert, K. Shen, P. Kota, S.M. Palmer, K.M. Plevock, A. Orlova, V.E. Galkin, K. Burridge, E.H. Egelman, et al. 2014. Identification of an actin binding surface on vinculin that mediates mechanical cell and focal adhesion properties. *Structure.* 22:697–706. http://dx.doi.org/10.1016/j.str.2014.03.002

Troyanovsky, S. 2012. Adherens junction assembly. *Subcell. Biochem.* 60:89–108. http://dx.doi.org/10.1007/978-94-007-4186-7_5

Troyanovsky, R.B., E.P. Sokolov, and S.M. Troyanovsky. 2006. Endocytosis of cadherin from intracellular junctions is the driving force for cadherin adhesive dimer disassembly. *Mol. Biol. Cell.* 17:3484–3493. http://dx.doi.org/10.1091/mbc.E06-03-0190

Troyanovsky, R.B., O. Laur, and S.M. Troyanovsky. 2007. Stable and unstable cadherin dimers: mechanisms of formation and roles in cell adhesion. *Mol. Biol. Cell.* 18:4343–4352. http://dx.doi.org/10.1091/mbc.E07-01-0084

Troyanovsky, R.B., J. Klingelhöfer, and S.M. Troyanovsky. 2011. α-Catenin contributes to the strength of E-cadherin-p120 interactions. *Mol. Biol. Cell.* 22:4247–4255. http://dx.doi.org/10.1091/mbc.E11-03-0250

Twiss, F., Q. Le Duc, S. Van Der Horst, H. Tabdili, G. Van Der Krogt, N. Wang, H. Rehmann, S. Huveneers, D.E. Leckband, and J. De Rooij. 2012. Vinculin-dependent Cadherin mechanosensing regulates efficient epithelial barrier formation. *Biol. Open.* 1:1128–1140. http://dx.doi.org/10.1242/bio.20122428

Vasioukhin, V., C. Bauer, M. Yin, and E. Fuchs. 2000. Directed actin polymerization is the driving force for epithelial cell-cell adhesion. *Cell.* 100:209–219. http://dx.doi.org/10.1016/S0092-8674(00)81559-7

Watabe-Uchida, M., N. Uchida, Y. Imamura, A. Nagafuchi, K. Fujimoto, T. Uemura, S. Vermeulen, F. van Roy, E.D. Adamson, and M. Takeichi. 1998. α-Catenin-vinculin interaction functions to organize the apical

junctional complex in epithelial cells. *J. Cell Biol.* 142:847–857. http://dx.doi.org/10.1083/jcb.142.3.847

Wu, Y., X. Jin, O. Harrison, L. Shapiro, B.H. Honig, and A. Ben-Shaul. 2010. Cooperativity between trans and cis interactions in cadherin-mediated junction formation. *Proc. Natl. Acad. Sci. USA.* 107:17592–17597. http://dx.doi.org/10.1073/pnas.1011247107

Yamada, S., S. Pokutta, F. Drees, W.I. Weis, and W.J. Nelson. 2005. Deconstructing the cadherin-catenin-actin complex. *Cell.* 123:889–901. http://dx.doi.org/10.1016/j.cell.2005.09.020

Yap, A.S., W.M. Brieher, M. Pruschy, and B.M. Gumbiner. 1997. Lateral clustering of the adhesive ectodomain: a fundamental determinant of cadherin function. *Curr. Biol.* 7:308–315. http://dx.doi.org/10.1016/S0960-9822(06)00154-0

Yonemura, S. 2011. Cadherin-actin interactions at adherens junctions. *Curr. Opin. Cell Biol.* 23:515–522. http://dx.doi.org/10.1016/j.ceb.2011.07.001

Yonemura, S., Y. Wada, T. Watanabe, A. Nagafuchi, and M. Shibata. 2010. α-Catenin as a tension transducer that induces adherens junction development. *Nat. Cell Biol.* 12:533–542. http://dx.doi.org/10.1038/ncb2055

Zhang, J., M. Betson, J. Erasmus, K. Zeikos, M. Bailly, L.P. Cramer, and V.M. Braga. 2005. Actin at cell-cell junctions is composed of two dynamic and functional populations. *J. Cell Sci.* 118:5549–5562. http://dx.doi.org/10.1242/jcs.02639